



UNIVERSITY OF LEEDS

This is a repository copy of *A new strategy for the relative movement of rough surfaces in contact using a boundary element method*.

White Rose Research Online URL for this paper:
<http://eprints.whiterose.ac.uk/100946/>

Version: Accepted Version

Article:

Ghanbarzadeh, A orcid.org/0000-0001-5058-4540, Wilson, M, Morina, A et al. (1 more author) (2016) *A new strategy for the relative movement of rough surfaces in contact using a boundary element method*. *European Journal of Computational Mechanics*, 25 (4). pp. 309-328. ISSN 1779-7179

<https://doi.org/10.1080/17797179.2016.1199237>

© 2016 Informa UK Limited, trading as Taylor & Francis Group. This is an Accepted Manuscript of an article published by Taylor & Francis in *European Journal of Computational Mechanics* on 20 June 2016, available online:
<http://www.tandfonline.com/10.1080/17797179.2016.1199237>. Uploaded in accordance with the publisher's self-archiving policy.

Reuse

Unless indicated otherwise, fulltext items are protected by copyright with all rights reserved. The copyright exception in section 29 of the Copyright, Designs and Patents Act 1988 allows the making of a single copy solely for the purpose of non-commercial research or private study within the limits of fair dealing. The publisher or other rights-holder may allow further reproduction and re-use of this version - refer to the White Rose Research Online record for this item. Where records identify the publisher as the copyright holder, users can verify any specific terms of use on the publisher's website.

Takedown

If you consider content in White Rose Research Online to be in breach of UK law, please notify us by emailing eprints@whiterose.ac.uk including the URL of the record and the reason for the withdrawal request.



eprints@whiterose.ac.uk
<https://eprints.whiterose.ac.uk/>

A New Strategy for the Relative Movement of Rough Surfaces in Contact Using a Boundary Element Method

Ali Ghanbarzadeh, Mark Wilson, Ardian Morina, Anne Neville

University of Leeds, School of Mechanical Engineering, Leeds, UK

Corresponding author:

E-mail address: a.ghanbarzadeh@leeds.ac.uk (Ali Ghanbarzadeh),

Abstract

Contact mechanics of rough surfaces is becoming increasingly important in understanding the real behaviours of machine elements in contact. Due to the complicated physical, chemical and mechanical phenomena occurring at surfaces especially in boundary lubrication, a multiphysics numerical model is essential to capture the behaviour. Boundary Element Method is a well-known numerical approach to model such a problem because of several advantages. Firstly it is far faster than Finite Element Method since only the boundaries of the solids are discretised. In addition, there is no problem of remeshing the contacting bodies due to plastic deformation and wear. Conventional Boundary Element models simulate movement of contacting surfaces by shifting matrices of numbers in one direction. In this new proposed approach, the big matrices of surfaces are cut into small matrices which indicate the part of surfaces that are in contact. The influence matrix is also cut into a smaller square matrix corresponding to the size of surface matrices. This approach enables matrix implications in smaller sizes than the original big surfaces and reduces the computational time.

Key words: contact mechanics, boundary element method, roughness, influence matrix

1. Introduction

Contact mechanics which explains the behaviour of materials in contact is of great importance since it occurs almost in all mechanical machine elements. In computational mechanics, Finite Element Method is a widely used approach to solve the contact problem. Robust formulations for contact and deformation of the solids are big advantages of FEM. Since the contact of solids is multiscale in nature, a multiscale computational analysis of the contact problem is essential.

Contact mechanics studies go back to 19th century when Hertz developed a model for a simple elastic contact (1). Hertz calculated contact pressure and deformation of an elastic contact. For this purpose a load was applied to surfaces and contact mechanics analysis started. As a result of load, each surface is

deformed by $u_i(x_1, x_2)$. A gap between surfaces was considered and Equation 1 should be satisfied in the contact:

$$u_1(x_1, x_2) + u_2(x_1, x_2) + g(x_1, x_2) = \delta_1 + \delta_2 \quad \text{Equation 1}$$

Hertz calculated the contact pressure of $p(x_1, x_2)$ in the case of satisfying the above equation.

Surfaces are rough in reality and contact of rough surfaces is more complicated than the Hertzian contact of flat surfaces. Because of the small scale of the roughness of the surfaces in compare to the bulk of the solids, Finite element Analysis of such a problem becomes cumbersome. One of the first attempts to mathematically solve the contact of rough surfaces was the work of Greenwood and Williamson (2). They used the probabilistic approach to predict the contact between surface asperities and determined the real area of contact. That model of contact mechanics was a starting point for understanding the real stochastic behaviour of surface asperities in contact. Despite the abilities of the model, it had no deterministic capabilities for measured surface topography.

Deterministic contact mechanics models have been the subject of many studies in the past few years to consider the true interaction of surface asperities in contact. Attempts were made on simulating the contact of surfaces using Finite Element Method. Bortoletto et al. (3) simulated a single ball-on-disc experiment by the finite element method and used Archard's wear equation to simulate wear. They validated the simulation results with experiments and showed good agreement. Oqvist (4) also used a finite element model to simulate a contact and implemented Archard's wear to calculate wear using an updated geometry with different step sizes.

Hegadekotte et al. (5) developed a multi-time-scale model for wear prediction in micro gear application. They used commercial codes for determining their contact pressure and deformations and then used Archard's wear equation for calculating wear. The problem of meshing size and remeshing the geometry was addressed in that work especially for the case of macro component wear calculations. Sellgren et al. (6) incorporated random rough surfaces into Finite Element analysis and calculated the true area of contact. They concluded that Finite

Element method can predict the real area of contact for rough surfaces. This prediction depends on the amplitude and wavelength properties of the interacting surfaces.

Boundary Element Method is also widely used for simulating the contact mechanics problem due to its efficiency. Sfantos et al. (7-9) developed boundary element simulations to calculate wear in sliding wear conditions. They reported that BEM is an efficient method for contact calculation of surfaces. They also used BEM for simulating the three dimensional sliding wear and validated the model with an artificial hip joint wear simulator.

Ilicic et al. (10-12) used the boundary element method and also a combined boundary-finite element method to simulate wear in tribometers using localized Archard's wear. They predicted the shape of the wear track of a flat surface in a reciprocating pin on disc tribometer using BEM. Anderson et al. (13) used a wear model and implemented FFT based contact mechanics simulations to calculate contact pressure and deformations. They simulated a ball on disc wear experiment and validated their simulation results with experiments.

There are several other works that simulate contact mechanics of rough surfaces using the Boundary Element Method for predicting wear and micropitting in rolling and rolling-sliding conditions (14-16). All these numerical procedures confirm that BEM is a suitable method for simulating contact mechanics.

Movement of surfaces are essential parts of any contact mechanics model that simulates sliding, rolling or sliding-rolling of contacting surfaces. In this work, a new numerical approach for movement of surfaces in contact mechanics simulations in Boundary Element Method is introduced. Instead of shifting the matrices containing the surface asperity height values, those parts of surfaces that come into contact are selected for contact mechanics simulation. The influence matrix is also modified with respect to the size of the part of the surfaces that are in contact. This approach helps to have smaller influence matrices and will increase the computational efficiency by several times. The details of the contact mechanics used in the Boundary Element simulation are also reported in this work. The contact mechanics model introduced in this work was used to investigate a boundary lubricated contact and tribochemistry in other works by the authors (17-19) and the predicting capability of the model was tested. In this paper, firstly, the components of the contact mechanics model is introduced in Section 2. The new strategy for the movement of the surfaces based on the new mathematical algorithm is presented in Section 2.5.1 . Then some examples of the results of the evolution of the asperity contact pressure is shown in Section 3.

2. Components of the model

2.1. Rough surface generation

To study the contact of rough surfaces deterministically, digitized surfaces should be used as inputs into the model. There are two different ways of digitizing surfaces. The first way is to use surface microscopes such as Atomic Force Microscope (AFM) which can give a 3D digitized map of the surface topography. Alternatively, surfaces can be generated using mathematical methods. The method used to generate surfaces is introduced by Hu et al. (20).

For generation of 3 dimensional rough surfaces, a specific autocorrelation factor and also height distribution should be defined. Two dimensional Digital filters are used for generating the 3 dimensional surfaces. By using random number generators it is possible to generate the filter inputs as Gaussian independent random numbers. The output would be obtained through the filtering operation and will give the sequence with certain autocorrelation function. It is mathematically proved that if the input numbers are Gaussian random numbers, the distribution will remain Gaussian after the filtering. The filtering coefficient for generating the rough surfaces is plotted in Figure 1. An example of 3D digitized rough surface is shown in Figure 2.

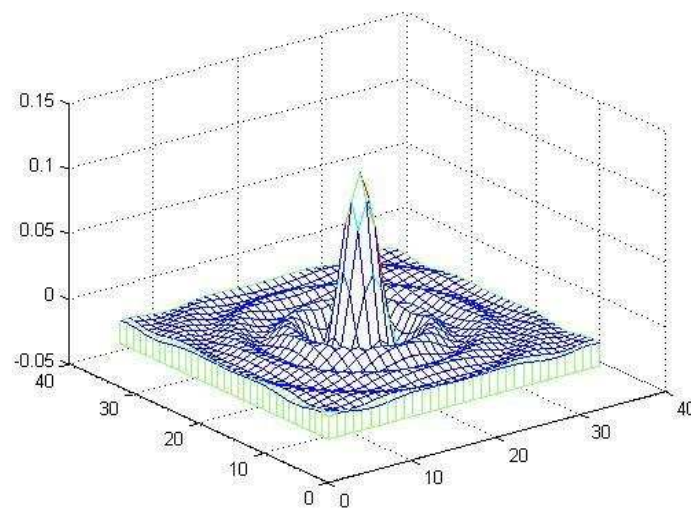


Figure 1 Filter coefficient for a circular digital low pass filter

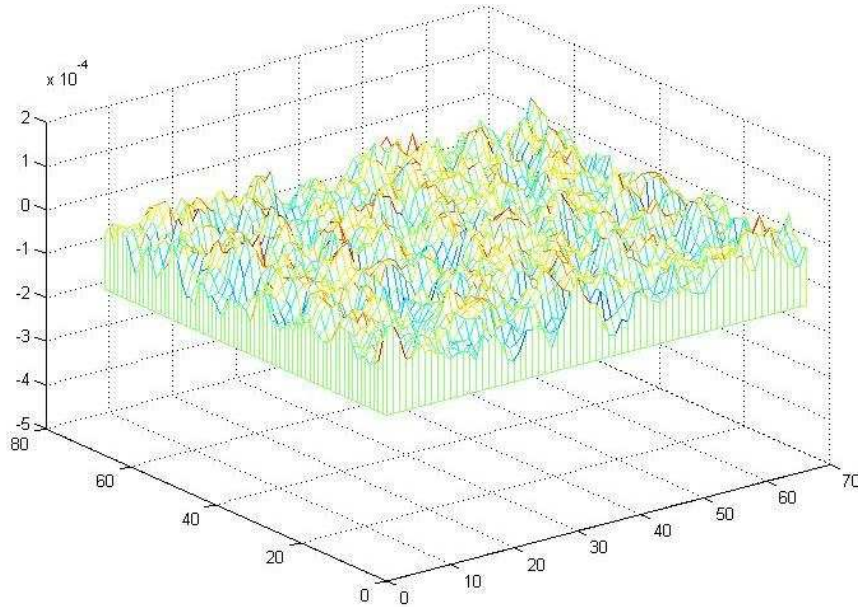


Figure 2 Three dimensional digital rough surface generated using low pass filter and random Gaussian numbers

This method enables varying surface roughness for studying the effect of roughness on contact of surfaces. As discussed before, surface roughness is very important in contact of surfaces in different scales, therefore this generation method gives the flexibility to generate different desired surfaces and investigating the surface effects in boundary lubrication.

2.2. Contact of rough surfaces

There have been many attempts at simulating the contact of rough surfaces in contact mechanics (6, 10-12, 21-30). The contact mechanics model developed by Tian and Bhushan (31) which considers the complementary potential energy will be used in this work. By applying the Boussinesq method (32) and relating the contact pressures to surface deformations, the problem would be to solve the contact mechanics only for finding contact pressures at each node and then the related contact deformations can be calculated. For this model, surfaces should be discretised into small nodes and it is assumed that the nodes are small enough and the contact pressure is constant at each node.

The problem is to minimize the complementary potential energy as follows:

$$V^* = \frac{1}{2} \iint p \bar{u}_z dx dy - \iint p \bar{u}_z^* dx dy \quad \text{Equation 2}$$

where p is the contact pressure and V^* , \bar{u}_z and \bar{u}_z^* are complementary potential energy, surface deformation and prescribed displacement respectively.

The Boussinesq solution for relating contact pressure and surface deformation usually considers only normal forces and the solution is:

$$u(x, y) = \frac{1}{\pi E^*} \iint_{-\infty}^{\infty} \frac{p(s_1, s_2)}{\sqrt{(x - s_1)^2 + (y - s_2)^2}} ds_1 ds_2 \quad \text{Equation 3}$$

in which E^* is the composite elastic modulus of two surfaces. (x, y) and (s_1, s_2) are two different surface points. It shows the relationship for the deformation of a the surface on point (x, y) when the load is applied on the point (s_1, s_2) .

$$\frac{1}{E^*} = \frac{(1 - \nu_1^2)}{E_1} + \frac{(1 - \nu_2^2)}{E_2} \quad \text{Equation 4}$$

$$\frac{1}{G^*} = \frac{(1 + \nu_1)(1 - 2\nu_1)}{2E_1} - \frac{(1 + \nu_2)(1 - 2\nu_2)}{2E_2} \quad \text{Equation 5}$$

Here, ν_1, ν_2, E_1 and E_2 are the Poisson's ratio and Elastic Modulus of surfaces 1 and 2 respectively.

For solving the double integrals of Equation 3 the surfaces should be discretised into small nodes. The nodes should be small enough to assume that pressure is constant at each node. It should be noted that only boundary of solids (surfaces) are meshed in this method which can help the numerical efficiency.

An example of the surface discretization is shown in Figure 3.

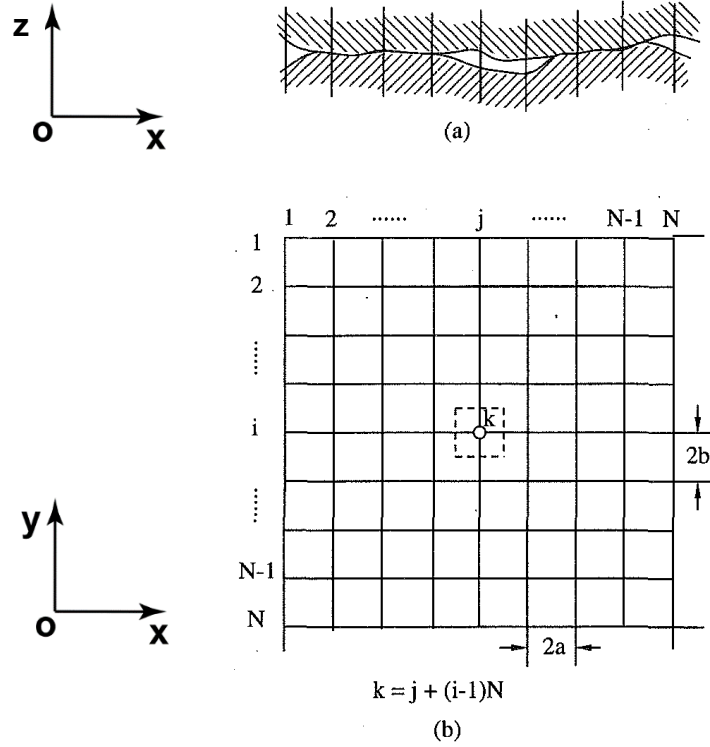


Figure 3 Surface discretization in Boundary Element Method (Reprinted from Ref (31))

N and M are the number of nodes in two dimensions of the surface plane and a and b are the half length of each element which is the difference between the nodes. For simplicity, a and b are assumed to be equal and in this work they are set to $0.5\mu\text{m}$. Therefore the full length of each element is $1\mu\text{m}$ which is a reasonable length for computational studies of rough surfaces (33).

To solve the integral equation for the discretised surfaces the integral equations should first be discretised.

$$\begin{aligned}
 (\bar{u}_z)_l &= \frac{1}{\pi E^*} \int_0^L \int_0^L \frac{p(s_1, s_2) ds_1 ds_2}{\sqrt{(s_1 - x)^2 + (s_2 - y)^2}} \\
 &= \frac{1}{\pi E^*} \sum_{k=1}^M \iint \frac{ds_1 ds_2}{\sqrt{(s_1 - x)^2 + (s_1 - y)^2}} p_k = \sum_{k=1}^M C_{kl} p_k
 \end{aligned}
 \tag{Equation 6}$$

C_{kl} is the influence matrix and is calculated by solving the double integral:

$$C_{kl} = \frac{1}{\pi E^*} \iint_{-\infty}^{\infty} \frac{ds_1 ds_2}{\sqrt{(x-s_1)^2 + (y-s_2)^2}} \quad \text{Equation 7}$$

The solution for the influence matrix in discretised form is as follows:

$$C_{kl} = \frac{1}{\pi E^*} \left\{ (x+a) \ln \left[\frac{(y+b) + \sqrt{(y+b)^2 + (x+a)^2}}{(y-b) + \sqrt{(y-b)^2 + (x+a)^2}} \right] \right. \\ + (y+b) \ln \left[\frac{(x+a) + \sqrt{(y+b)^2 + (x+a)^2}}{(x-a) + \sqrt{(y+b)^2 + (x-a)^2}} \right] \\ + (x-a) \ln \left[\frac{(y-b) + \sqrt{(y-b)^2 + (x-a)^2}}{(y+b) + \sqrt{(y+b)^2 + (x-a)^2}} \right] \\ \left. + (y-b) \ln \left[\frac{(x-a) + \sqrt{(y-b)^2 + (x-a)^2}}{(x+a) + \sqrt{(y-b)^2 + (x+a)^2}} \right] \right\} \quad \text{Equation 8}$$

in which a and b are the half-length of each small element and M is the total number of nodes.

Equation 2 describes the potential energy for a frictionless contact and the normal force is the only force applied on the surfaces. The potential equation for a frictional contact would be modified to the form below:

$$V^* = \frac{1}{2} \iint t \bar{u} dx dy - \iint t \bar{u}^* dx dy \quad \text{Equation 9}$$

In which \mathbf{t} is the full surface stress vector including the in-plane tractions and \mathbf{u} is the full surface deformation.

$$\mathbf{t} = q_x \mathbf{e}_x + q_y \mathbf{e}_y + p \mathbf{e}_z \quad \text{Equation 10}$$

$$\mathbf{u} = u_x \mathbf{e}_x + u_y \mathbf{e}_y + u_z \mathbf{e}_z \quad \text{Equation 11}$$

q_x and q_y are the in-plane traction forces and \mathbf{e}_x , \mathbf{e}_y and \mathbf{e}_z are the Cartesian unit basis vectors.

u_x , u_y and u_z are the surface deformations in x, y and z directions respectively.

By applying the same discretising procedure, the Boussinesq solution for the fully coupled deformation-traction relationship can be expressed as:

$$\begin{aligned}
 u_{xk} &= \sum_{l=1}^M (C_{kl}^{xx} q_{xl} + C_{kl}^{xy} q_{yl} + C_{kl}^{xz} p) \\
 u_{yk} &= \sum_{l=1}^M (C_{kl}^{yx} q_{xl} + C_{kl}^{yy} q_{yl} + C_{kl}^{yz} p) \\
 u_{zk} &= \sum_{l=1}^M (C_{kl}^{zx} q_{xl} + C_{kl}^{zy} q_{yl} + C_{kl}^{zz} p)
 \end{aligned}
 \tag{Equation 12}$$

In the matrix form:

$$\begin{bmatrix} u_x \\ u_y \\ u_z \end{bmatrix} = \begin{bmatrix} C^{xx} & C^{xy} & C^{xz} \\ C^{yx} & C^{yy} & C^{yz} \\ C^{zx} & C^{zy} & C^{zz} \end{bmatrix} \begin{bmatrix} q_x \\ q_y \\ p \end{bmatrix}
 \tag{Equation 13}$$

The elements of the influence matrix can be obtained from the complete solution of the Boussinesq problem. Then the problem would be minimizing the potential energy for the fully coupled contact. The solution procedure is the same as frictionless contact and can be carried out by direct quadratic mathematical solution (31, 34).

For the case of two identical materials in contact, the equivalent shear modulus of Equation 5 becomes zero and the Equation 9 reduces to Equation 3.

2.3. Direct quadratic mathematical programming

Because the total complementary potential energy is a quadratic function of the contact pressure, it can be expressed as quadratic mathematical equations. Hence the energy can be written in quadratic form of Equation 14:

$$V^* = \frac{1}{2} p^T \cdot C \cdot p - p^T u
 \tag{Equation 14}$$

Here p^T is the transpose matrix of p_k and C and u are influence matrix and gap between surfaces respectively.

$$C = \frac{1}{\pi E^*} \begin{bmatrix} C_{1,1} & \cdots & C_{1,M} \\ \vdots & \ddots & \vdots \\ C_{M,1} & \cdots & C_{M,M} \end{bmatrix} \quad \text{Equation 15}$$

$$u^T = (\overline{u_{z1}^*}, \overline{u_{z2}^*}, \dots, \overline{u_{zk}^*}, \dots, \overline{u_{zM}^*}) \quad \text{Equation 16}$$

And for the complementary potential energy to have a minimum at the point p^* , the solution is as:

$$\begin{aligned} \nabla V^*(p^*) &= C \cdot p^* - u = 0 \\ p^* &= C^{-1} \cdot u \end{aligned} \quad \text{Equation 17}$$

And all the values in Equation 17 should satisfy the restriction criteria $p_k \geq 0$. The summation of all contact pressures must be equal to the applied load on the surfaces and the following equation should be satisfied:

$$\sum_{i,j=1}^{i,j=N} p_{i,j} = W \quad \text{Equation 18}$$

The elastic deformation is then calculated corresponding to the pressure of contacting asperity using the equation below:

$$u = C \cdot p \quad \text{Equation 19}$$

The deformation is then used to check the deformation criteria of the contact problem. It should be noted that Equation 18 will be valid for the whole contact. In order to find the true area of contact and the corresponding contact pressures, Equation 18 and Equation 20 should be solved at the same time iteratively.

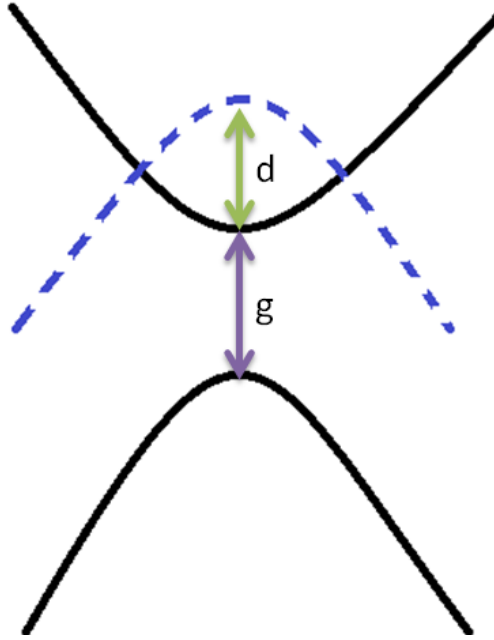


Figure 4 Single asperity model – Schematics of rigid body movement

The rigid body movement (r) is the movement of the bodies in normal direction of contact and is given by:

$$\begin{aligned}
 r &= (Z_2 - Z_1) + u \quad \& \quad p > 0 \quad \text{if in contact} \\
 r &< (Z_2 - Z_1) + u \quad \& \quad p = 0 \quad \text{if not in contact}
 \end{aligned}
 \tag{Equation 20}$$

in which $(Z_2 - Z_1) = g$ is the gap between asperities and u is the elastic deformation of contacting asperities. The above formulations are valid for every single asperities in contact. Therefore they can be solved for a set of asperities and Figure 4 can be a representative of a single node in the contact mechanics formulation of the problem explained in Figure 3

2.4. Elastic-perfectly plastic contact model

The contact mechanics model used in this work is an elastic-perfectly plastic model. To consider the plastic part in the simulation, a modelling approach which was reported by Sahlin et al. (35) was used in this work. It is assumed that the asperities can undergo pressures between 0 and hardness of the materials:

$$0 < p(x, y) < H$$

Equation 21

The contact pressure of the asperities that experience pressures higher than the hardness of the materials will be set to H (hardness of the material).

These asperities become plastically deformed. It is assumed that the points with pressures equal to the hardness of the material will be truncated out of the calculation for elastic deformation because they can freely float. The steps for elasto plastic contact simulation are explained as below:

- First step is to guess the initial pressure to satisfy Equation 18.
- Set the negative pressures to zero and the pressures above the hardness to H
- Check the calculated pressures again and compare it with Equation 18. If the pressure is now equal to load, pressures should be shifted up or down
- Truncate the pressures $p = 0$ and $p = H$. Then calculate the elastic deformation of Equation 19.
- Calculate the body interferences and check if the points of contact will satisfy Equation 20.
- The plastic deformation is then calculated by subtracting the elastic deformation from the body interferences.

2.5. Movement of the contacting surfaces

The influence matrix of Equation 15 shows the influence of surface points on deformation of other points in presence of load. The term g which is a two dimensional matrix of gaps between single asperities of contacting surfaces, shows the potential of asperity-asperity contact by moving surfaces in normal direction of surface planes. In this case Equation 20 defines the possibility of contact to happen.

In most of the tribologically loaded contacts, surfaces have relative movements tangentially, so this must be taken into account. Conventionally, movement of surfaces are applied by shifting the matrices that contain the surface asperity height numbers. This is a very simple way to simulate the movement of surfaces. In this method controlling the shifting speed of both contacting surfaces is essential for applying the rolling-sliding condition on the tribosystem.

The influence matrix does not change in this method and the size is still $(N * M) \times (N * M)$ which in the case of square contacting area becomes $N^2 \times N^2$.

2.5.1 New surface movement strategy

It is important to know how the influence matrix works before explaining the new procedure for moving the surfaces. The elements of an influence matrix correspond to the influence of a node of surface on other nodes of the surface if the load is applied on that point.

Imagine a surface with $N \times N$ nodes. If the load is applied to a point, it influences $N \times N$ points on the surfaces including the point itself. Therefore, a matrix of $N^2 \times N^2$ can explain the influence matrix of the whole surface. Each element of this matrix is responsible for the influence of a point on another point (Figure 5). If the load is applied on point p it will affect the deformation on point k.

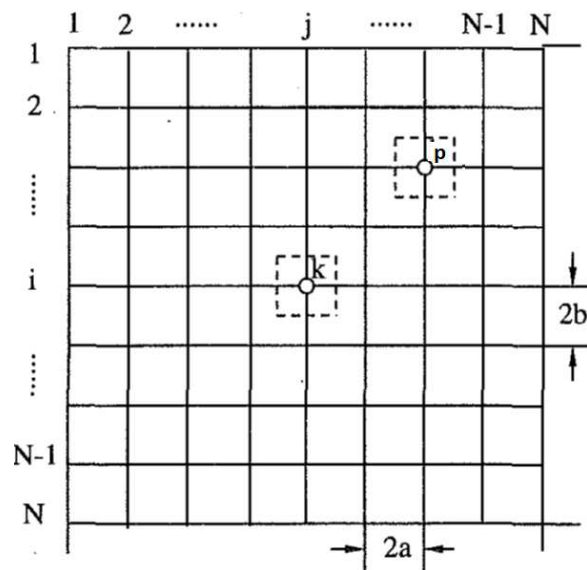


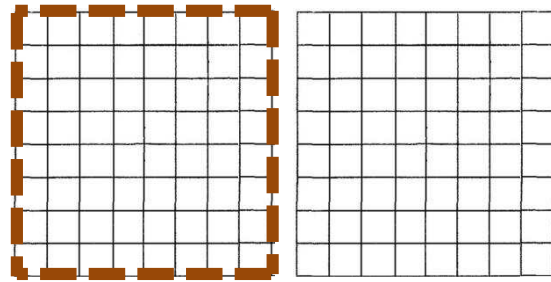
Figure 5 Discretized surface and influence matrix definition

It can be interpreted from Equation 8 that the elements of this matrix are dependent on the distance of the points on the surface (distance between points p and k). Therefore, this matrix would have identical values for the points that have similar distances.

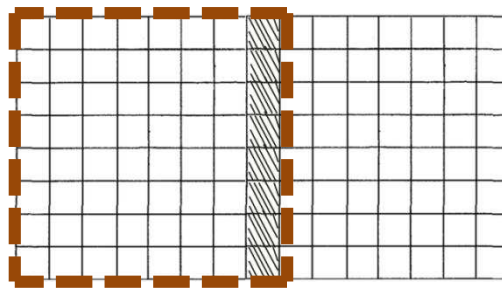
Now imagine two surfaces coming into rolling-sliding contact. One of the surfaces should enter the contact from one side and will exit the contact on the opposite.

If the upper surface enters the contact from the left, its rightmost part would be in contact with the leftmost part of the lower surface (Figure 6-b). Then the contact problem reduces to the

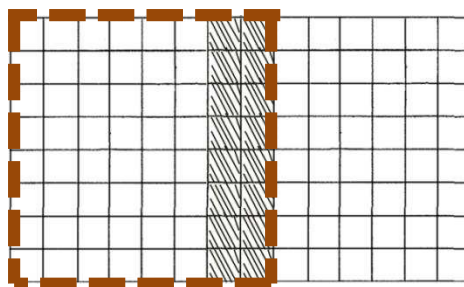
contact of two one-dimensional matrices of two surfaces with size $(N \times 1)$. When the movement continues, more points of surfaces come into contact. For example two columns of the rightmost points of upper surface come into contact with two columns of the leftmost points on the lower surface (Figure 6-c). This process continues until the surfaces fully come into contact and the upper surface exits the contact from the other side. A schematic of this contact process is shown in Figure 6.



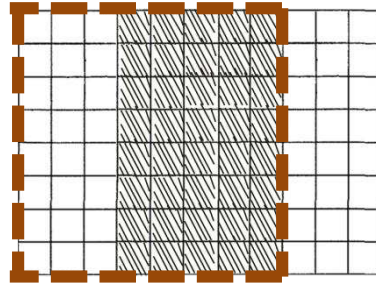
a) Two surfaces not in contact yet



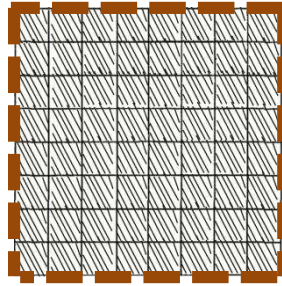
b) Start of the contact (rightmost part of a surface in contact with leftmost part of another surface)



c) Two surfaces come into contact by more areas of both surfaces



d) More evolution in the contact area of surfaces



e) Entire surfaces are in contact

Figure 6 Movement of surfaces in contact. The shaded area shows the area of contact between two surfaces. The red dotted lines shows the area of the upper surface that enters the contact from the left.

For the beginning of the contact one column of each surface comes into contact. In this case, the influence matrix needs to cover the contact of N points on one surface with N points on another surface. Therefore the influence matrix only needs to be the first $N \times N$ matrix of the big $N^2 \times N^2$ influence matrix. It is shown in Figure 7 that how this $N \times N$ matrix is selected.

The true influence matrix elements should satisfy Equation 8. As stated before, these elements are dependent on the distance of the points of the surface so the selection shown in Figure 7 is valid.

If the movement continues and more points of the surfaces come into contact, the influence matrix will get bigger and becomes $2N \times 2N$, $3N \times 3N$, ... and $N^2 \times N^2$ at the end when surfaces are completely in contact.

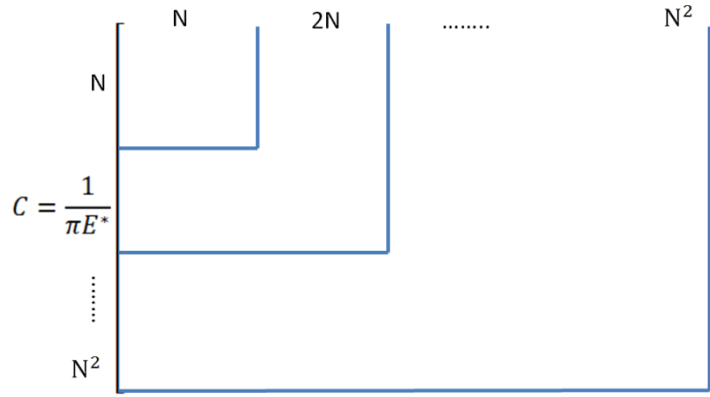


Figure 7 Influence matrix selection in the case of moving surfaces

The problem of contact becomes faster because the size of matrices of surfaces and influence matrices are much smaller in this case. The maximum size of the influence matrix is when two surfaces are in complete contact and it is the same size as conventional shifting of surfaces. It should be noted that the rigid body movement (r) is set as constant in one entire step of the contact calculation (from when the surfaces come into the contact up until the surfaces exit the contact). The average of the surface contact pressures are taken in one step and this value is used to satisfy Equation 18. In this case, upper surface is passed relative to the lower surface and the average of the contact pressure is calculated on surface asperities and the calculation is iterated until it satisfies Equation 18 and Equation 20.

Then the contact pressures and surface deformations are stored for every step and can be averaged for one loading cycle. Plastic deformations are applied to the surface asperities and the geometries of the surfaces are changed for next steps. This process of two rough surfaces coming into contact is repeated to the end of the simulation. Therefore a rolling sliding motion can be easily modelled by this contact mechanics simulation. It should be noted that the contact mechanics model in this work is quasi-static.

3. Results and discussion

Results for influence matrix and contour of contact pressure for movement of surfaces are reported in this section.

3.1. Influence matrix

As explained before influence matrix is $N^2 \times N^2$ when the surfaces are $N \times N$. An example of influence matrix for a 20×20 surface is shown in Figure 8.

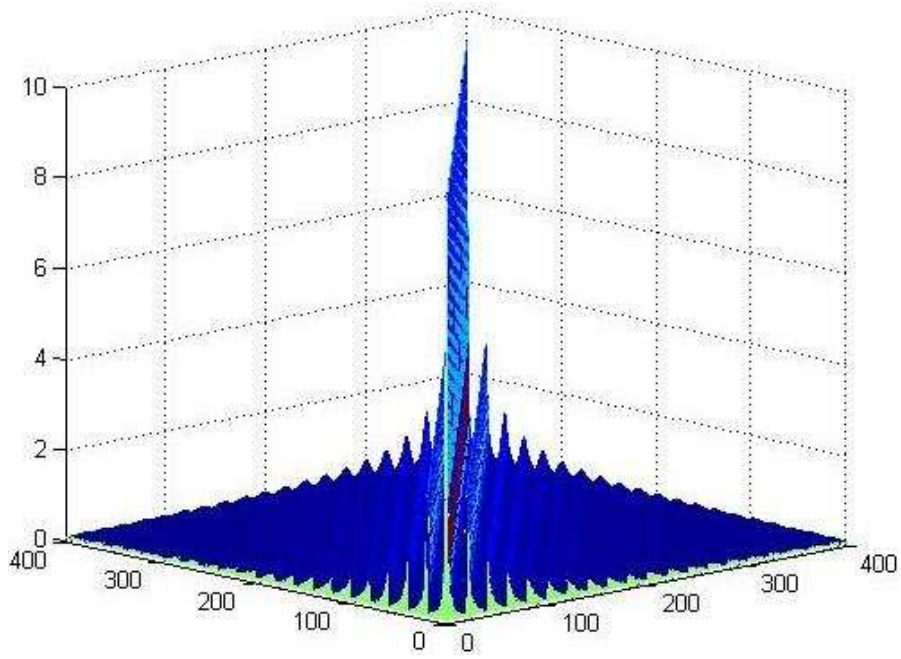


Figure 8 Influence matrix element values

If load is applied to a point of this surface, the deformation on all the other points is shown in Figure 9.

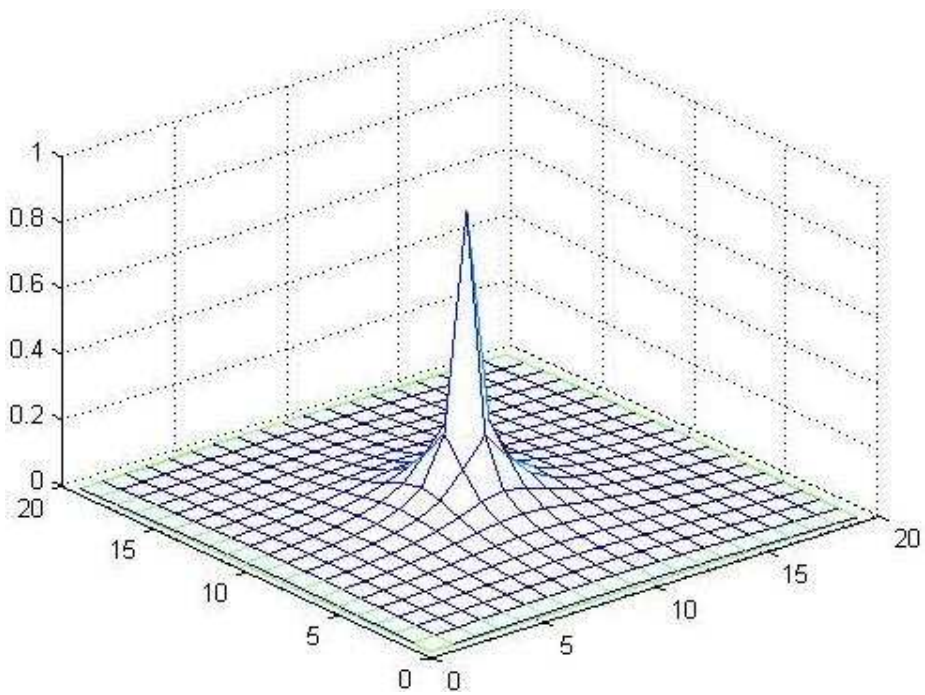


Figure 9 The deformation of surface due to load applied in the centre

It is noticeable that if a load is applied to a certain point on the surface, the highest deformation happens at the same point and this deformation decreases as the distance from that point increases. It is in agreement with the definition of the influence matrix.

Figure 8 shows the elements of influence matrix and it approves the fact that selection of matrix elements based on Figure 7 is valid. By selecting the first $N \times N$ matrix of the large $N^2 \times N^2$ influence matrix, the influence of one point of the surface on the 20 points of the same column is selected. That is for the case that surfaces are only at the beginning of the contact.

It can be also noted that the influence matrix of Figure 8 is diagonal which means that the influence element of all points are the same on themselves and is reduced by the distance of the points from each other. It is also symmetric diagonally which means that the same distance between the points results in the same influence value.

3.2. Movement of the surfaces

As explained in section 2.5. , matrices of surfaces are selected in a way that movement can be simulated. An example of this movement is shown in Figure 10. The contour of contact pressure which shows the asperity-asperity interaction is demonstrated in the figure. The evolution of contacting asperities in the sliding direction can be noticed from the figure.

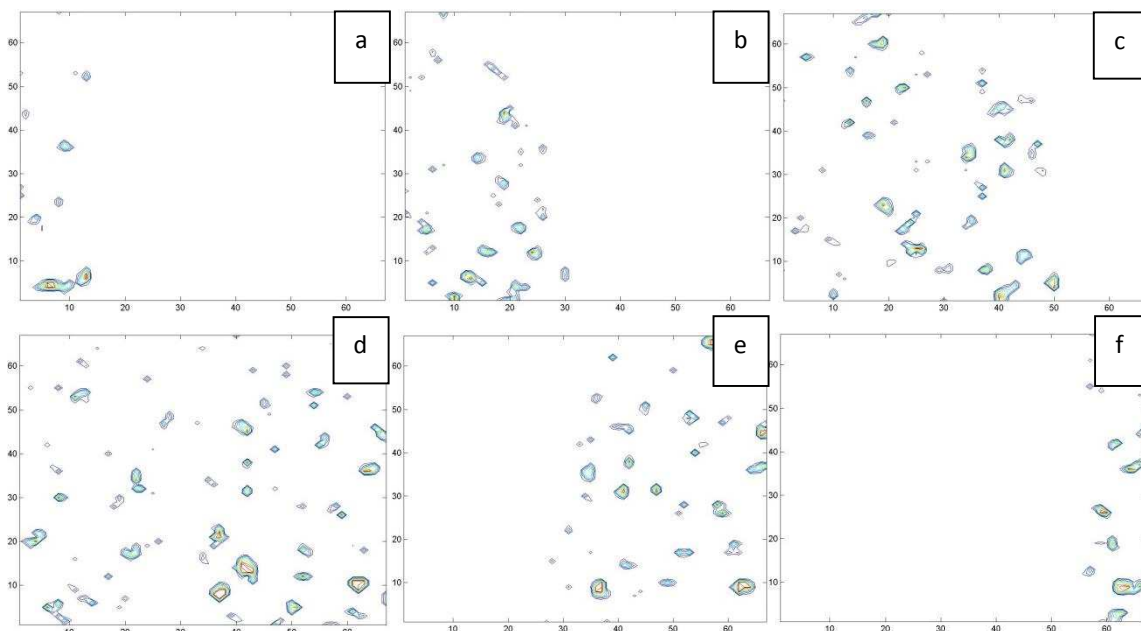


Figure 10 Contour of contact pressure showing the asperity contact pressures in surface movement. The upper surface enters the contact from the left (a) and exits from the right (f). The contour is indicating the pressures on the lower body.

The upper surface comes into contact with lower surface from the left (see Figure 10-a) and moves towards the sliding direction. Both surfaces are entirely in contact in Figure 10-d. The upper surface then exits the contact from the other side (Figure 10-f).

The influence matrix is smaller in the beginning of the contact (Figure 10-a) and increases in size whilst more surface points come into contact. It gets the size of the original influence matrix while two surfaces are completely in contact (Figure 10-d) and then reduces in size as the upper surface start to exit the contact.

3.3. Application in non-linear contact problems

Non-linear contact problems have been the subject of many studies. Models focused on incorporating non-linear behavior in finite element methods, boundary element methods and combination of them two (36-45).

Any contact problem will be no longer a linear one due to yielding of the materials in contact. The stress can be calculated at any loading increment as the following:

$$[\Delta\sigma] = [D_{ep}] \cdot [\Delta\varepsilon] \quad \text{Equation 22}$$

Where $[\Delta\varepsilon]$ is the strain increment and $[D_{ep}]$ is the elasto-plastic influence matrix. It is shown numerically that the stress fields and the contact deformations in an elastio-plastic non-linear problem can be calculated using the influence matrices used for elastic problems with a more complicated numerical algorithm (45). Results show that calculation of non-linear problems need the influence matrix or the stiffness matrix for pressure/deformation calculations. However, these numerical results are for the contact of material in a normal loading without any tangential movements. Therefore, the movement methodology shown in Section 2.5.1 is applicable for movement of surfaces in the case of non-linear contact problems. The only change in the numerical approach would be adapting the influence/stiffness matrices to account for the part of the surfaces that are in contact.

4. Conclusion

Boundary Element Method is an efficient approach for simulating the contact mechanics especially in the case of rough surfaces. Tribological contacts are dynamic and surfaces are in relative motion in contact. These dynamic conditions will result in modification to geometry and physics of the contacting bodies. Modelling such a problem needs a robust and efficient

algorithm for movement of surfaces. A new algorithm for movement of surfaces in Boundary Element Method was reported in this work. In this approach, parts of the surfaces are selected out of the bigger real area of contact and the corresponding influence matrix is extracted from the original influence matrix. A big advantage of this approach is the smaller sizes of influence matrix for contacts. The computation time of a contact mechanics simulation is directly proportional to size of the influence matrix. The contact mechanics results shown in this work are similar to the ones reported in the literature. This approach can be also used for the non-linear contact problems by adapting the influence/stiffness matrices in a way that only account for the part of the surface that are in contact. Influence/stiffness matrices can be modified for each loading increments in the non-linear problem. Smaller matrices can increase the efficiency of the non-linear problems by several times.

5. Acknowledgement

This study was funded by the FP7 program through the Marie Curie Initial Training Network (MC-ITN) entitled “ENTICE - Engineering Tribochemistry and Interfaces with a Focus on the Internal Combustion Engine” [290077] and was carried out at University of Leeds.

References

1. Hertz H. On the contact of elastic solids. *J reine angew Math.* 1881;92(156-171):110.
2. Williamson JAGaJBP. Contact of Nominally Flat Surfaces. *Proceedings of the Royal Society of London A Mathematical and Physical Sciences.* 1966;295(1442).
3. E.M. Bortoleto ACR, V.Seriacopi,F.J.Profitto,D.C.Zachariadis,I.F.Machado,, A. Sinatora RMS. Experimental and numerical analysis of dry contact in the pin on disc test. *Wear.* 2012;301(1):19-26.
4. Öqvist M. Numerical simulations of mild wear using updated geometry with different step size approaches. *wear.* 2001;249(1):6-11.
5. V. Hegadekatte J. Hilgertb OKNH. Multi time scale simulations for wear prediction in micro-gears. *Wear.* 2010;268(1):316-24.
6. Sellgren U, Björklund S, Andersson S. A finite element-based model of normal contact between rough surfaces. *Wear.* 2003;254(11):1180-8.
7. G.K. Sfantos MHA. Application of BEM and optimization technique to wear problems. *International journal of solids and structures.* 2006;43(11):3626-42.
8. G.K. Sfantos MHA. Wear simulation using an incremental sliding Boundary Element Method. *Wear.* 2006;260(9):1119-28.
9. Sfantos G, Aliabadi M. A boundary element formulation for three-dimensional sliding wear simulation. *Wear.* 2007;262(5):672-83.
10. Ilincic S, Tungkunagorn N, Vernes A, Vorlaufer G, Fotiu P, Franek F. Finite and boundary element method contact mechanics on rough, artificial hip joints. *Proceedings of the Institution of Mechanical Engineers, Part J: Journal of Engineering Tribology.* 2011;225(11):1081-91.
11. Ilincic S, Vernes A, Vorlaufer G, Hunger H, Dörr N, Franek F. Numerical estimation of wear in reciprocating tribological experiments. *Proceedings of the Institution of Mechanical Engineers, Part J: Journal of Engineering Tribology.* 2013;227(5):510-9.
12. Ilincic S, Vorlaufer G, Fotiu P, Vernes A, Franek F. Combined finite element-boundary element method modelling of elastic multi-asperity contacts. *Proceedings of the Institution of Mechanical Engineers, Part J: Journal of Engineering Tribology.* 2009;223(5):767-76.
13. J. Andersson AA, R. Larsson. Numerical simulation of a wear experiment. *Wear.* 2011;271(11):2947-52.
14. Bosman R, Schipper DJ. Running-in of systems protected by additive-rich oils. *Tribology Letters.* 2011;41(1):263-82.
15. Bosman R, Schipper DJ. Mild Wear Prediction of Boundary-Lubricated Contacts. *Tribology Letters.* 2011;42(2):169-78.
16. Morales-Espejel GE, Brizmer V. Micropitting modelling in rolling–sliding contacts: Application to rolling bearings. *tribology transactions.* 2011;54(4):625-43.
17. Ghanbarzadeh A, Wilson M, Morina A, Dowson D, Neville A. Development of a New Mechano-Chemical Model in Boundary Lubrication. *Tribology International.* 2016;93:573-82.
18. Ghanbarzadeh A, Parsaeian P, Morina A, Wilson MC, van Eijk MC, Nedelcu I, et al. A Semi-deterministic Wear Model Considering the Effect of Zinc Dialkyl Dithiophosphate Tribofilm. *Tribology Letters.* 2016;61(1):1-15.
19. Ghanbarzadeh A, Piras E, Nedelcu I, Brizmer V, Wilson MCT, Morina A, et al. Zinc Dialkyl Dithiophosphate Antiwear Tribofilm and its Effect on the Topography Evolution of Surfaces: A Numerical and Experimental Study. *Wear.* 2016.
20. Tonder YZHaK. Simulation of 3-D random rough surface by 2-D digital filter and Fourier analysis. *International journal of machine tools and manufacture.* 1992;32(1):83-90.
21. A. Almqvist FS, R. Larsson, S. Glavatskih. On the dry elasto-plastic contact of nominally flat surfaces. *Tribology international.* 2007;40(4):574-9.
22. b RATaWB. A Model for Asperity Load Sharing in Lubricated Contacts. *ASLE transactions.* 1972;15(1):67-79.

23. Bhushan B. Contact mechanics of rough surfaces in tribology: multiple asperity contact. *Tribology Letters*. 1998;4(1):1-35.
24. Borri-Brunetto M, Chiaia B, Ciavarella M. Incipient sliding of rough surfaces in contact: a multiscale numerical analysis. *Computer Methods in Applied Mechanics and Engineering*. 2001;190(46-47):6053-73.
25. Conry TF, Seireg A. A mathematical programming method for design of elastic bodies in contact. *Journal of Applied Mechanics*. 1971;38:387.
26. Kalker J, Van Randen Y. A minimum principle for frictionless elastic contact with application to non-Hertzian half-space contact problems. *Journal of engineering mathematics*. 1972;6(2):193-206.
27. Lai W, Cheng H. Computer simulation of elastic rough contacts. *ASLE transactions*. 1985;28(2):172-80.
28. Ren N, Lee SC. Contact simulation of three-dimensional rough surfaces using moving grid method. *Journal of tribology*. 1993;115(4):597-601.
29. Poon C, Sayles R. Numerical contact model of a smooth ball on an anisotropic rough surface. *Journal of tribology*. 1994;116(2):194-201.
30. Webster M, Sayles R. A numerical model for the elastic frictionless contact of real rough surfaces. *Journal of tribology*. 1986;108(3):314-20.
31. Xuefeng Tian BB. A Numerical Three-Dimensional Model for the Contact of Rough Surfaces by Variational Principle. 1996.
32. K.L.Johnson. *Contact Mechanics*.
33. Joel Andersson, Roland Larsson, Andreas Almqvist, Grahnb M, Minami I. Semi-deterministic chemo-mechanical model of boundary lubrication. *faraday Discussions*. 2012;156(1):343-60.
34. Willner K. Fully coupled frictional contact using elastic halfspace theory. *Journal of Tribology*. 2008;130(3):031405.
35. F Sahlin RL, A Almqvist, P M Lugt and P Marklund. A mixed lubrication model incorporating measured surface topography. Part 1: theory of flow factors. *Proceedings of the Institution of Mechanical Engineers, Part J: Journal of Engineering Tribology*. 2009;224(4):335-51.
36. Andersson T. The boundary element method applied to two-dimensional contact problems with friction. *Boundary element methods: Springer*; 1981. p. 239-58.
37. Kosior F, Guyot N, Maurice G. Analysis of frictional contact problem using boundary element method and domain decomposition method. *International journal for numerical methods in engineering*. 1999;46(1):65-82.
38. Landenberger A, El-Zafrany A. Boundary element analysis of elastic contact problems using gap finite elements. *Computers & structures*. 1999;71(6):651-61.
39. Man K, Aliabadi M, Rooke D. BEM frictional contact analysis: load incremental technique. *Computers & structures*. 1993;47(6):893-905.
40. Man K, Aliabadi M, Rooke D. BEM frictional contact analysis: modelling considerations. *Engineering analysis with boundary elements*. 1993;11(1):77-85.
41. Olukoko O, Becker A, Fenner R. A new boundary element approach for contact problems with friction. *International journal for numerical methods in engineering*. 1993;36(15):2625-42.
42. Oysu C, Fenner R. Two-dimensional elastic contact analysis by coupling finite element and boundary element methods. *The Journal of Strain Analysis for Engineering Design*. 1998;33(6):459-68.
43. Yamazaki K, Sakamoto J, Takumi S. Penalty method for three-dimensional elastic contact problems by boundary element method. *Computers & structures*. 1994;52(5):895-903.
44. Ezawa Y, Okamoto N. Development of contact stress analysis programs using the hybrid method of FEM and BEM. *Computers & structures*. 1995;57(4):691-8.
45. Liu G, Zhu J, Yu L, Wang QJ. Elasto-Plastic Contact of Rough Surfaces. *Tribology transactions*. 2001 2001/01/01;44(3):437-43.